European Journal of Medicinal Chemistry 45 (2010) 5397–5405

Contents lists available at ScienceDirect

European Journal of Medicinal Chemistry

journal homepage: http://www.elsevier.com/locate/ejmech

Original article

Phenylmethylene hydantoins as prostate cancer invasion and migration inhibitors. CoMFA approach and QSAR analysis

Mohammad A. Khanfar, Khalid A. El Sayed*

Department of Basic Pharmaceutical Sciences, College of Pharmacy, University of Louisiana at Monroe, 1800 Bienville Drive, Monroe, Louisiana 71201, USA

ARTICLE INFO

Article history:
Received 2 July 2010
Received in revised form
27 August 2010
Accepted 27 August 2010
Available online 8 September 2010

Keywords:
Phenylmethylene Hydantoins
Anti-invasion
Prostate cancer
CoMFA
QSAR

ABSTRACT

Prostrate cancer constitutes the second leading cause of cancer deaths in men in United States. In the process of discovery of new antiproliferative and anti-metastatic agents against prostate cancer, marine-derived phenylmethylene hydantoin (PMH) derivatives were identified with activity level range between 50 and 200 μM. 3D-QSAR CoMFA model was used in virtual screening of commercially available derivatives of PMH. PMH derivatives with manifold increase in anti-migratory and anti-invasive activities were discovered using wound-healing and Cultrex invasion assays. Benzene ring replacement with other heterocyclic rings did not significantly improve the methylene hydantoins activities. Multivariate analysis performed on the whole series of methylene hydantoins, which further supported the findings of CoMFA model. Predictive QSAR model with conventional r^2 and cross-validated coefficient (q^2) values up to 0.982 and 0.803 were established. The molecular volume (MV) and the log *P* were identified as critical parameters for methylene hydatoins migration inhibitory activity. PMH is a novel anti-metastatic lead class with potential therapeutic activity against prostate cancer.

1. Introduction

Prostate cancer remains the leading cause of men's mortality worldwide [1]. Despite important progress in the early diagnosis of prostate neoplasias through the measurement of prostate-specific antigen levels, 10% of newly diagnosed patients have some evidence of locally advanced prostate cancer and 5% already have distant metastasis at the time of diagnoses [2,3]. Postmortem analysis of deaths attributed to prostate cancer reveals that most subjects have evidence of metastatic disease [4]. Some treatment alternatives exist with limited curative potential in the case of locally advanced prostate cancer [5–7]. In contrast, patients with evidence of distant metastasis have very poor prognosis and no curative treatment exists [8]. Prostate cancer deaths are a result of metastatic disease and treatment of such metastatic disease is one of the major therapeutic challenges. Thus, there is urgent need to develop novel therapeutic approaches and strategies to control metastatic prostate cancer.

Over the past few years, hydantoin derivatives have attracted a great attention due to their diverse biological activities. These include fungicidal, herbicidal, anti-inflammatory, anti-HIV, analgesic, cannabinoid receptor-1, 5HT, purine P-2X receptor antagonism, platelet aggregation inhibition, anti-arrhythmic and antihypertensive, anti-diabetic, neuroprotective, HDL/cholesterol modulating, antiviral, anticonvulsant, and growth hormone secretagogue [9,10]. On the other hand, much interest has been given to their cancer chemotherapeutic activity. Hydantoins were shown to inhibit MMPs [11] and were patented in 1987 for their tyrosine kinase inhibitory and antiallergic activities [12]. 2-[4-[(5-Oxo-2-thioxo-4-imidazolidinylidene)-methyl]phenoxy] propionic acid and analogs bind the ERK1 or ERK2 kinase, inhibit phosphorylation, and slow cell proliferation in vitro [13]. Peptide hydantoin analogs were patented for their ability to inhibit thrombocyte aggregation, metastasis, and osteoclast binding to bone surfaces [14]. A β-carboline hydantoin was found to have phosphodiesterase 5 and colon tumor cell growth inhibition activity [15]. 5-Benzylidene hydantoins inhibited A549 lung cancer cell line proliferation via dual mechanism; inhibiting EGFR autophosphorylation and increasing p53 level [16]. Azaspiro bicyclic hydantoin derivatives have anti-tumor and anti-angiogenic activity against ovarian and osteosarcoma cells through down regulation of the secretion of VEGF [17]. Substituted hydantoin derivatives have also been patented as MEK1 and MEK2 inhibitors, which are useful targets in the treatment of cell proliferative disorders including cancer [18]. Fluorinated spirohydantoin derivative induced cytotoxicity in chronic myelogenous leukemia by inhibiting the cell growth via interfering with DNA replication [19]. Hydantoin derivatives were found to have androgen receptor modulation, which can be used for treating prostate cancer and other androgen receptor-related

* Corresponding author. Tel.: +1 318 342 1725; fax: +1 318 342 1737.
E-mail address: elsayed@ulm.edu (K.A. El Sayed).

0223-5234/$ – see front matter © 2010 Elsevier Masson SAS. All rights reserved.
doi:10.1016/j.ejmech.2010.08.066

diseases [20]. Phenylemthylene hydantoins (PMH) were reported to inhibit GSK-3β, potential target for the treatment of cancer, Alzheimer's disease, bipolar disorders, and type-2 diabetes [21].

Natural products have proven to be the most reliable source of new anticancer entities [22,23]. Nearly 63% of anticancer drugs introduced over the last 25 years are natural products or can be traced back to a natural products origin [24]. A recent review lists 79 natural products or natural product analogs that entered clinical trial as anticancer agents between 2005 and 2007 [25]. Ethanolic extract of the abundant shallow water Red Sea sponge *Hemimycale arabica* inhibited the proliferation and invasion of the highly metastatic human prostate cancer PC-3M cell line [26,27]. Liquid chromatography of this extract afforded the known (*Z*)-5-(4-hydroxybenzylidene)-hydantoin (**1**) [27]. This natural PMH (**1**) and the related synthetic (*Z*)-5-(4-(ethylthio)benzylidene)-hydantoin (**2**) showed potent in-vitro anti-growth and anti-invasive properties against PC-3M prostate cancer cells in MTT and spheroid disaggregation assays [26,27]. PMHs **1** and **2** also showed anti-invasive activity in orthotopic xenograft of PC-3 M cells in nude mice model [26]. They decreased orthotopic tumor growth and inhibited the formation of tumor micrometastases in distant organs without apparent cytotoxic effects at the test doses [23]. PMH **2** also showed a potent activity in LPB-Tag mice transgenic model [26]. PMH **2** remarkably reduced growth of primary tumors and their metastasis in reproductive organs, decreased morbidity and increased survival of the LPB-Tag mice [26]. Recently, **1** and **2** were found to decrease total CD44 and CD44 v7–10 expression, which could partly explain their anti-metastatic activity [21].

Previous study from our laboratory has investigated the influence of substitutions in the phenyl ring of the PMH on the prostate cancer migration inhibitory activity [27]. Using regioselective and cost-effective condensation reaction of hydantoin and substituted benzaldehyde, several diverse derivatives of PMH molecule that exhibit different degrees of activity were structurally modified [27]. On the basis of this investigation, predictive 3D-QSAR (CoMFA) model with conventional r^2 and cross-validated coefficient (q^2) values up to 0.910 and 0.651 were established [27]. The main objective of this study is to further discover and optimize new PMH derivatives with enhanced anti-migratory and anti-invasive activities against prostate cancer cells. To accomplish this aim, three strategies were applied. Firstly, CoMFA-based virtual screening of in-house database of virtually sketched PMHs using all benzaldehydes that are commercially available in Sigma–Aldrich and VWR repositories was conducted. Since all structural modifications in the first report were focused on the substitutions of the phenyl ring of PMH, the second applied strategy was the investigation of the influence of replacing the phenyl ring with other heterocyclic rings. Finally, predictive quantitative structure-activity relationship (QSAR) was derived based on the relevant physiochemical descriptors of the compounds that would be of value in guiding lead PMH design. The partial least square (PLS) method was applied to find relationships between the in vitro activity and the physiochemical data.

2. Results and discussion

2.1. Chemistry

PMHs were synthesized using Scheme 1 [9]. This Scheme includes base-catalyzed condensation of hydantoin with substituted benzaldehydes [28]. Geometrical isomerism (*E*/*Z* isomers) was possible due to the restricted rotation around the exocyclic $\Delta^{5,6}$ double bond of the PMHs, however this method regioselectively afforded the *Z*-geometry as confirmed by the spectral data. The IR spectra of PMHs showed the stretching vibration bands at a higher frequency region (1660–1675 cm^{-1}) characteristic for *Z*-oriented $\Delta^{5,6}$ bonds, which are distinguishable from those expected for the *E* isomers (1630–1640 cm^{-1}) [9]. The chemical shift of the most diagnostic olefinic proton H-6 was downfield shifted in the ^1H NMR spectra (δ_H 6.40–7.00), which further confirmed the *Z*-orientation of the $\Delta^{5,6}$ system. The expected chemical shift of H-6 in the *E* isomers should be 6.20–6.30 ppm. The downfield shift of H-6 in the *Z* isomer is attributed to the anisotropic effect of the spatially nearby C-4 carbonyl group [9].

2.2. Virtual screening and biological evaluation

3D-QSAR model of 35 PMH derivatives was generated and validated using Comparative Molecular Field Analysis (CoMFA) [27]. Predictive 3D-QSAR model with conventional r^2 and cross-validated coefficient (q^2) values up to 0.910 and 0.651, respectively, were established [27]. CoMFA steric and electrostatic fields from PLS analysis were generated [27]. In this analysis both steric and electrostatic fields contribute to the QSAR equation by 70.6% and 29.4%, respectively [27]. This suggested that variation in biological activity of inhibitors is dominated by differences in steric (van der Waals) interactions with the hydantoins active site.

Virtual screening (VS) has been a fruitful strategy for lead identification for several decades. Its use has substantially increased in recent years, especially with the advent of online databases, ending the discovery of new hits out of millions of virtual structures. VS offers means to systematically select a small number of compounds, which can then be tested in lower-throughput assays, increasing the likelihood of discovery and identification of compounds with desired activities as compared to the more-expensive and time-consuming physical high-throughput screening. The study herein applied ligand-based virtual screening using the validated CoMFA model to design and discover new PMH derivatives with enhanced anti-migratory and anti-invasive activities (Fig. 1). All commercially available substituted benzaldehydes in VWR and Sigma–Aldrich repositories were collected and the corresponding PMH derivatives were virtually sketched using SYBYL 8.0. 636 virtual PMH derivatives were subjected to CoMFA (PLS) model and predicted cutoff IC_{50} value of 50 μM was used as selection criteria. Eighteen PMH derivatives were found to have calculated IC_{50} less than 50 μM, but only 15 were readily available for synthesis (Table 1). All compounds were first tested at 100 μM in wound-healing assay against the metastatic prostate cancer (PC-3) and compounds with percentage inhibition ≥50% were further tested to determine their IC_{50} values (Table 1). Five compounds (**3**, **4**, **7**, **9**, and **10**) exhibited potent anti-migratory activity, including compound **10** with 5-folds better activity compared to the lead PMH **2**. Compound **10** (IC_{50} = 8.1 μM) showed a strong inhibition of PC-3 migration in dose–response manner in wound-healing assay (Fig. 2) without significant cytotoxicity up to 200 μM as assessed by the MTT assay. Working consistently with CoMFA model, the common feature between the five most active compounds is the presence of bulky aliphatic and aromatic substitution at the *para*-position of the phenyl ring although they have different electronic properties.

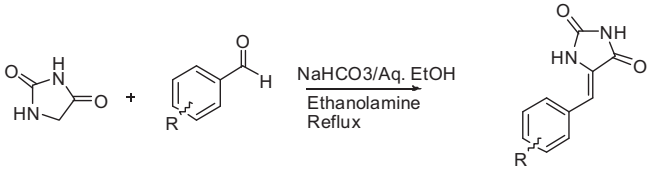

Scheme 1. General synthetic scheme of phenylmethylene hydantoins.

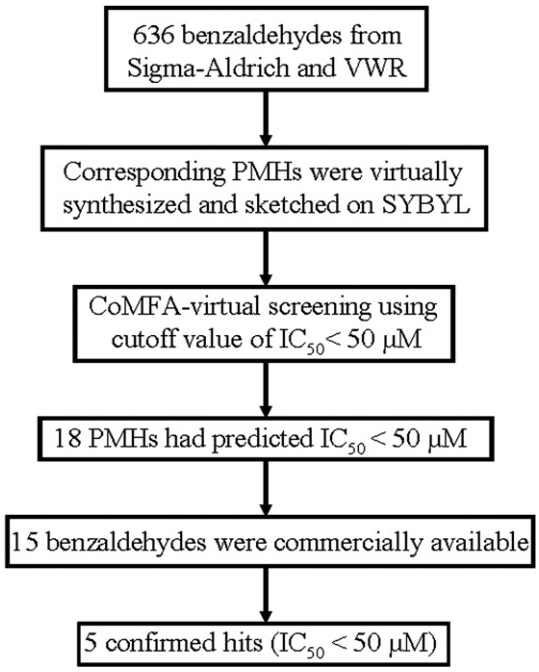

Fig. 1. Outlines of the virtual screening methodology that was applied to discover new active PMHs.

Bioisosteric replacement of the phenyl ring of PMH with other heterocyclic ring was attempted (Fig. 3). Excluding compound **21**, replacement of the phenyl with other heteroaromatic functionality did not improve the anti-migratory activity relative to the lead **2**. Bioisosteric replacement of the thioethane moiety in **2** with a thiophene in **21** showed a good anti-migratory activity in wound-healing assay ($IC_{50} = 32.5$ μM) and equipotent activity to the lead **2** ($IC_{50} = 42.9$ μM).

Anti-invasive activities of active compounds in wound-healing assay (**2**–**4**, **7**, **9**, **10**, **12**, **13**, **21**) were measured using Trevigen's Cultrex® 96 well Basement Membrane Extract (BME) cell invasion assay kit against the highly metastatic PC-3 cells [28,29]. This assay employs a simplified Boyden Chamber design with a polyethylene terephthalate membrane (8 μm). Detection of cell invasion is quantified using calcein-AM [28,29]. Cells internalize calcein-AM and intracellular esterases cleave the acetomethylester moiety to generate free calcein. Free calcein fluoresces brightly, and this fluorescence may be used to quantify the number of cells that have invaded across BME [28,29]. Anti-invasive activities of **2**–**4**, **7**, **9**, **10**, **12**, **13**, and **21** at 50 μM doses are shown in Fig. 4. Comparable to wound-healing assay, PMH **10** was 5-folds more active than the hit PMH **2**. Other active PHMs also showed variable range of activities. Interestingly, PMH **21** was 3-folds more potent than **2**, though it was equipotent in wound-healing assay, suggesting multiple targets for this compound. Active compounds were then tested for their cytotoxic activity using MTT assay (Fig. 5). Excluding **13**, PMHs did not display any significant cytotoxicity against PC-3 over 72 h at the maximum tested dose (200 μM). This shows a clear difference between the cytotoxic and anti-invasive activity levels. Different derivatives of PMH were tested in vivo for their anticonvulsant [9] and GSK-3β inhibitory [21] activity using maximal electroshock seizure and liver-glycogen level, respectively. These compounds were well tolerated with no reported fatalities. These in-vivo and in-vitro data presented herein provide a preliminary indication of excellent safety and tolerability of PMHs as active entity. The high activity and low cytotoxicity of **10** could provide a basis for designing new analogs with wide therapeutic window. Future modification of compound **10** may be required to enhance its potency to nanomolar activity, while maintaining its low cytotoxicity.

Table 1
Structures of PMHs and their biological activities in wound-healing assay against PC-3 cells.

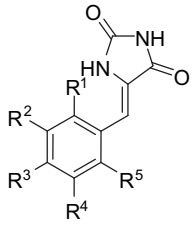

Cmpd	R^1	R^2	R^3	R^4	R^5	% Inhibition at 100 μM	IC_{50}[a]
1	H	H	OH	H	H	34	127.9 ± 8.1
2	H	H	SEt	H	H	42.9 (at 50 μM)	42.9 ± 4.7
3	H	H	OCH_2(4-F-Ph)	H	H	76.3	23.8 ± 3.3
4	H	Br	OEt	OEt	H	77.5	35.7 ± 1.5
5	H	OMe	OCH_2CO-pyrrolidine	H	H	36.3	86 ± 10.1
6	OPr	H	OPr	H	H	68.4	77.1 ± 4.0
7	H	H	OCH_2COPh	OMe	H	91.8	19.7 ± 2.9
8	H	H	OCH_2CO-mopholine	H	H	33.2	94 ± 11.7
9	H	Cl	OCH_2CCH	OMe	H	88.8	21.8 ± 3.5
10	H	OMe	OPr	Br	H	97.4	8.1 ± 1.4
11	H	H	$OCH_2CH_2CH(CH_3)_2$	H	H	66.7	46.1 ± 8.0
12	H	H	pyrrolidine	H	H	75.9	48.7 ± 6.1
13	H	H	SMe	H	H	80.9	44.7 ± 9.3
14	OMe	H	OPr	H	H	23	110 ± 12.3
15	OMe	Cl	OtBu	H	H	39	91 ± 7.8
16	OMe	Cl	OPr	H	OMe	19	187 ± 17.9
17	H	H	OtBu	H	H	52.7	60.8 ± 4.9

[a] The values are the mean ± SD. Each experiment was conducted in triplicate.

Overall activities profile of PMHs showed that long bulky substituents with various aliphatic or aromatic groups at the *para*-position of the benzene ring are favorable with manifold increase in anti-migratory and anti-invasive activities. This finding is confirmed by QSAR analysis, as described later. Alternatively, electron-donating substitution on one *meta*-position and electron-withdrawing on the other *meta*-position with limited steric properties are associated with activity improvement. However, *ortho*-substituent is not tolerable, which dramatically decreases the activity.

2.3. QSAR analysis

Multivariate analysis was carried out on all the methylene hydantoins which were characterized by 14 physicochemical descriptors representing various size, electronic, and lipophilic properties (Supporting Information Table 1). The lipophilicity of the methylene hydantoins was described by theoretically-determined log *P* (clog *P*) values and number of hydrophobic center (HC). The size parameters of methylene hydantoins were described by molecular volume (MV), molecular area (MA), bond counts (BC), molar refractivity (MR), and polar surface area (PSA). The electronic properties of hydantoins were described by the dipole moment (DM), highest occupied molecular orbital (HOMO), lowest unoccupied molecular orbital (LUMO), hydrogen bond acceptor (HBA), hydrogen bond donor (HBD), and ionization potential (IP). All physiochemical parameters were theoretically calculated using the SYBYL 8.0 spreadsheet autofill module [30]. The difference in ^{13}C

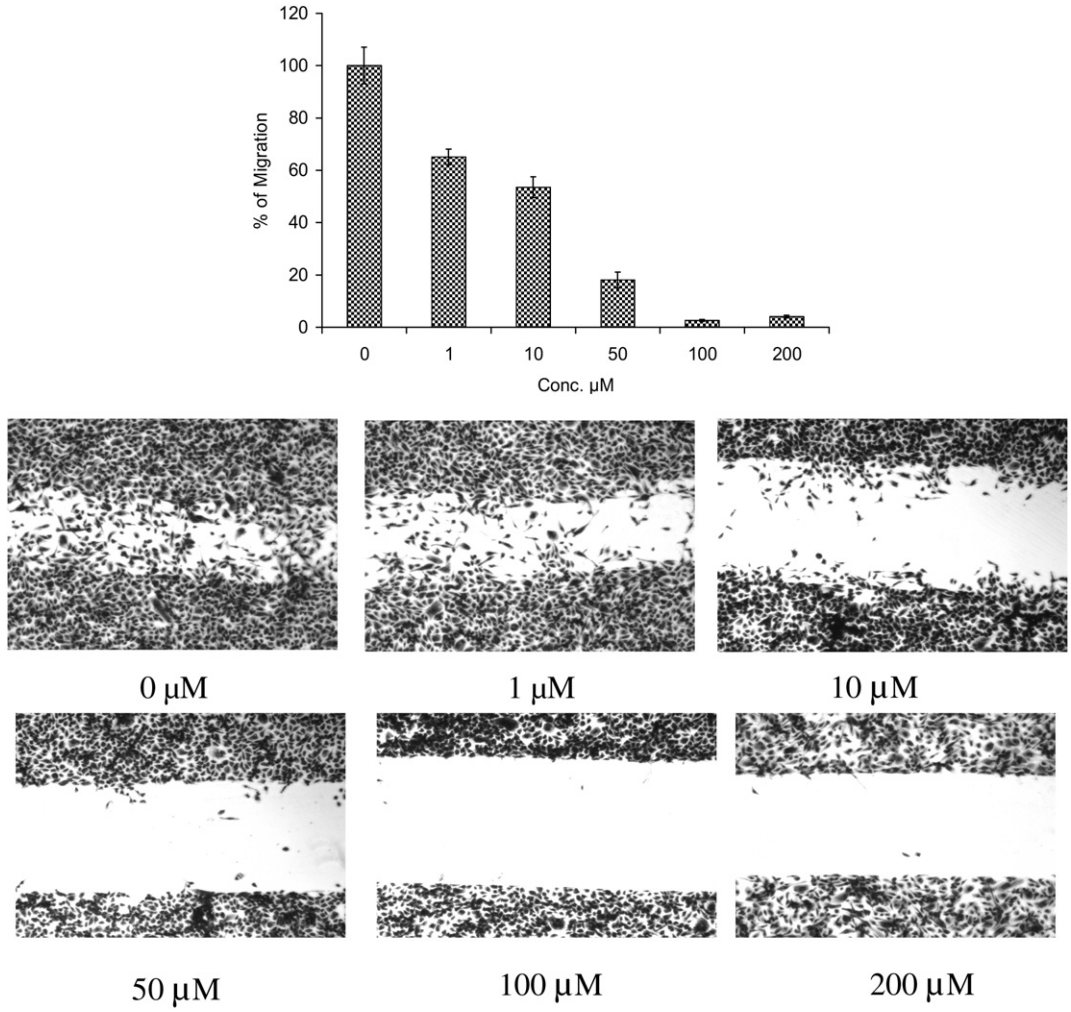

Fig. 2. Dose–response activity of **10** in wound-healing assay against PC-3 cell line. Magnification = 100×.

chemical shift ($\Delta\delta$), an additional electronic parameter, was experimentally determined by NMR studies.

Principal component analysis (PCA) was used to evaluate the molecular diversity of the methylene hydantoins selected for the QSAR study [31]. The partial least squares projection to latent structures (PLS), which is a regression extension of PCA, was later used to quantify and predict the relationship between the activity and physicochemical descriptors [31]. It was imperative to evaluate

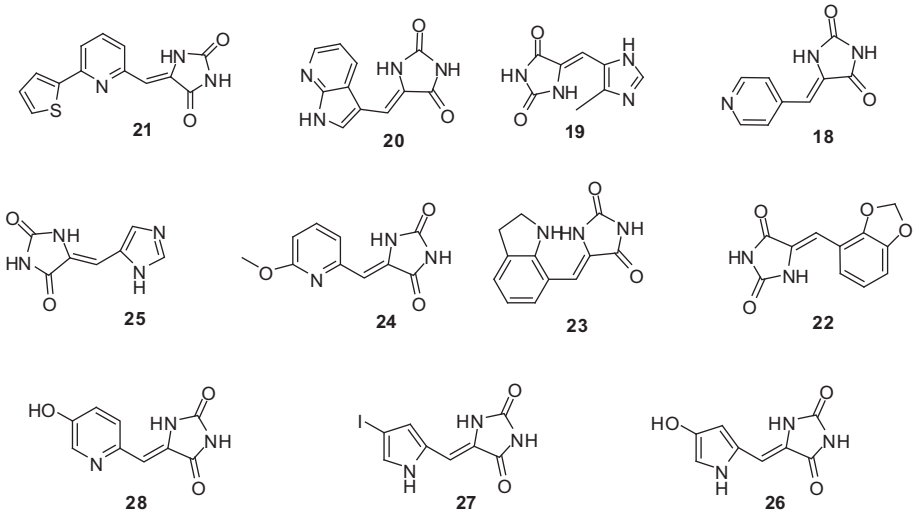

Fig. 3. Structural modification of PMH using different heterocycles.

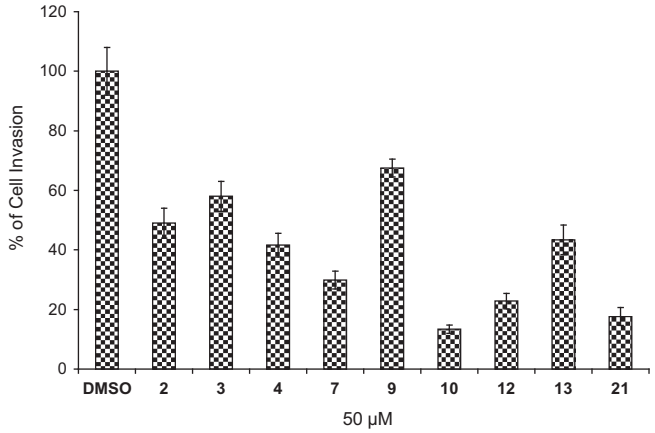

Fig. 4. Anti-invasive activities of PMHs against PC-3 cells using Cultrex™ assay kit. Error bars indicate the SD of $n = 3$/concentration.

the predictivity of the generated QSAR models. The molecules were divided into training and test sets. Selection of the training set and the test set compounds was done by considering the fact that test set compounds represent a range of biological activity similar to that of the training set. Thus, the test set was a true representative of the training set. This was achieved by arbitrarily setting aside five compounds as a test set with a regularly distributed biological data. The mean (standard deviation) of the activity of the training and test sets was 77.92 (50.12) and 85.02 (63.93), respectively. Table 2 shows the actual and predicted activity for both training and test sets. Twenty-three hydantoins were used to build these QSAR models. The IC_{50} (concentration causing 50% inhibitory effect on the PC-3 migration) values were converted to pIC_{50} ($-\log IC_{50}$) values and used as dependent variables in the analysis.

PLS analysis of all of the compounds in the training set and using all the 14 descriptors resulted in a QSAR model with a moderate cross-validated correlation coefficient (q^2) value of 0.474 and conventional correlation coefficient (r^2) value of 0.849 (model 1, Table 3). Earlier reports stated that models with q^2 greater than 0.5 were considered to have predictive capability better than chance, and with higher q^2, higher reliability could be attained [31]. Hence, the model was further refined to improve q^2 and in turn its predictive power. On the basis of the relative importance, out of 14 physicochemical descriptors, some might not significantly contribute to the activity, and hence, it was decided to exclude the less important ones from the analysis to improve the predictive power of the model. The variable importance projection (VIP) plot is a measure of the relative importance of variables included in the analysis with respect to their contribution to the activity. Descriptors with a VIP value greater than 1 were considered to have above-average influence on the activity [31].

Inspection of the VIP plot showed little contribution from many descriptors. HOMO, LUMO, IP, HBA, PSA, DM, and ^{13}C chemical shift difference were found to be less important because their VIP plot values were less than 1 (Fig. 6). The exclusion of these descriptors improved the model and accounted for 95% and predicted 76% of the anti-migratory activity of the methylene hydantoins (model 2, Table 3). Examination of the residuals from the LOO cross-validated predictions indicated that compound **27** might be an outlier. Omission of this compound resulted in an increase in the q^2 value to 0.803 for the remaining 22 compounds (model 3, Table 3). The outlier status of **27** could stem from the presence of an electron-withdrawing bulky iodine atom attached to the pyrrole ring. One would expect a higher potency for **27** than it exhibited based on the significant importance of MV to the activity. This analysis predicted the activities of the compounds of test set with predictive correlation coefficient (r^2_{Pred}) of 0.574. Fig. 7 shows the plot of the predicted versus observed activities of the training and test sets.

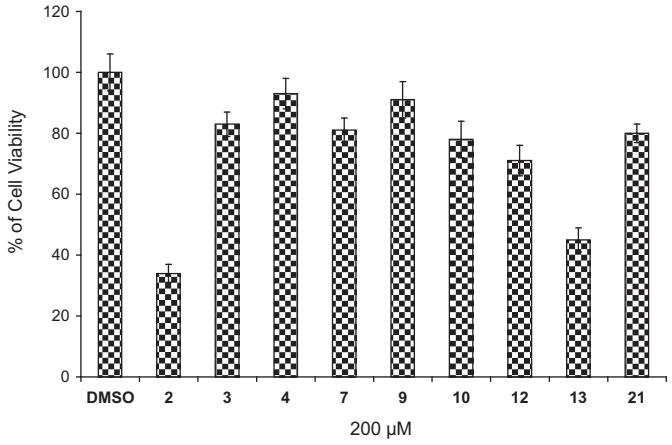

Fig. 5. Cytotoxic activity of PMHs at 200 μM against PC-3 using MTT assay. . Error bars indicate the SD of $n = 3$/concentration.

Table 2
Experimental and predicted pIC_{50} of the training and test sets.

Compound	Actual pIC_{50}[a]	Pred. pIC_{50}[b]	Sets
1	−2.106	−2.321	Training
2	−1.632	−1.638	Training
3	−1.376	−1.22	Training
4	−1.552	−1.495	Training
5	−1.934	−1.953	Training
6	−1.887	−1.991	Test
7	−1.294	−1.639	Test
8	−1.973	−1.900	Training
9	−1.338	−1.403	Training
10	−0.908	−0.884	Training
11	−1.663	−1.292	Test
12	−1.687	−1.682	Training
13	−1.650	−1.865	Training
14	−2.041	−2.002	Training
15	−1.959	−1.909	Training
16	−2.271	−2.666	Test
17	−1.783	−1.753	Training
18	−2.251	−2.281	Training
19	−1.978	−1.689	Test
20	−1.696	−1.463	Training
21	−1.511	−1.599	Training
22	−2.189	−1.902	Training
23	−1.937	−1.931	Training
24	−1.777	−1.573	Training
25	−1.734	−1.881	Training
26	−1.996	−2.045	Training
27	−2.299	−2.175	Training
28	−1.913	−1.908	Training

[a] pIC_{50} (-logIC_{50}) values were experimentally tested in the wound-healing assay in PC-3 cells.
[b] Predicted pIC_{50} from the QSAR model 3.

Table 3
Summary of PLS models developed for PMHs by the QSAR analysis.

Model description	No. of components[a]	q^2	r^2	n[b]	No. of descriptors	RMSEE[c]
Model 1	4	0.474	0.849	23	14	0.052
Model 2	3	0.757	0.954	23	7	0.008
Model 3	3	0.803	0.982	22	7	0.005

[a] Number of significant components obtained in the PLS analysis.
[b] Number of compounds used in the analysis.
[c] Root-mean-square error of estimation in the analysis (predicted vs observed).

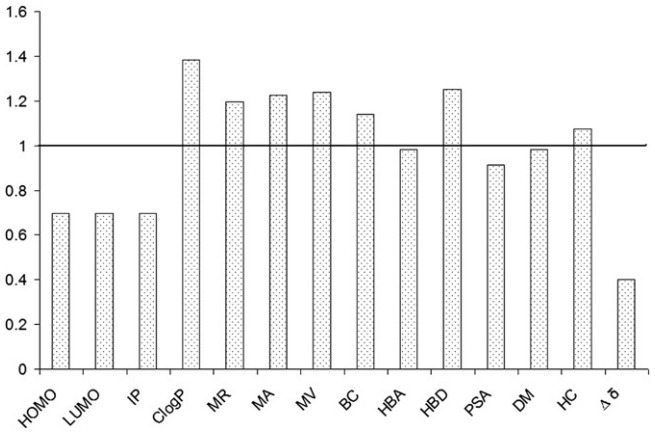

Fig. 6. VIP Plot from PLS analysis of data in model 1 (Table 3).

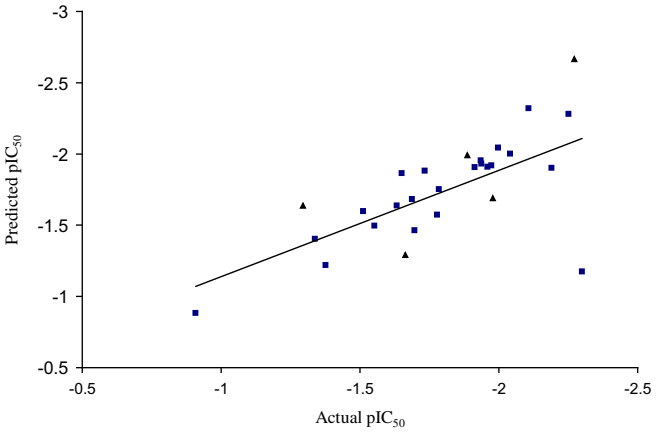

Fig. 7. Actual versus calculated pIC_{50} of PMHs as predicted from model 3 (■, training set, ▲, test set).

A careful inspection of VIP plot and descriptor's correlation coefficients in model 3 revealed the importance of both size and lipophilic parameters. The descriptors were found in the order of increasing importance: MA < MV < BC < clog *P*. The MV, BC, and clog *P* were directly related to the activity, while MA was inversely related (Eq. (3) in the Supporting Information). All other electronic parameters such as HOMO, LUMO, DM were less contributing according to model 1 and VIP plot. Based on the VIP and model 3 (Fig. 6 and Supporting Information Eq. (3)), the most influential two descriptors were found to be clog *P* and MV. This is expected because many of the active methylene hydantoins have lipophilic and bulky substituents especially at the *para*-position of the benzylidene moiety (e.g., hydantoins **3**, **7**, **9**, and **10**). These findings are strongly correlated with the CoMFA model, where the steric contribution to activity variation was 70.6% [27].

3. Conclusions

In this study, we present a successful example of employing CoMFA-based virtual screening to identify new PMH derivatives with enhanced anti-migratory and anti-invasive activities. A set of 15 PMHs were selected from the virtual 635 compounds for biological testing. New PMHs with manifold increase in the activity were identified with modest efforts and expenses by screening only 15 PMHs, highlighting an important feature of the virtual screening approach. QSAR study using multivariate analysis gave a significant PLS model that could account for 98% and predict 80% of their anti-migratory activity. The model demonstrated the significance contribution of the size and lipophilicity on the activity of methylene hydantoins. PMH is a novel anti-metastatic lead class that can be easily, regioselectively, and cost-effectively synthesized. These advantages bode well for the emergence of future PMHs as potential therapeutics for the control and prevention of metastatic prostate cancer.

4. Experimental section

4.1. General experimental procedures

The ^1H and ^{13}C NMR spectra were recorded in d_6-DMSO, using TMS as an internal standard, on a JEOL Eclipse NMR spectrometer (Tokyo, Japan) operating at 400 MHz for ^1H and 100 MHz for ^{13}C. The HREIMS experiments were conducted in Louisiana State University on a 6200-TOF LCMS (Agilent, Santa Clara, CA) equipped with a multimode source (mixed source that can ionize the samples alternatively by ESI and APCI). Analytical HPLC analyses were performed on a Shimadzu HPLC system (Columbia, MD) using Agilent 5μ C18 Column (150 × 4.6 mm id; Agilent, Santa Clara, CA), and isocratic elution (CH_3CN-H_2O, 75:25) with UV detection set at 305 and 220 nm to verify the purity of each tested compound. A purity of >98% has been established for all compounds. TLC analyses were carried out on precoated Si gel 60 F_{254} 500 μm TLC plates, using MeOH-CH_2Cl_2 (2:8) as a developing solvent.

4.2. Preparation of phenylmethylene hydantoins

Hydantoin (0.1 g) was dissolved in 1 mL H_2O while heating at 70 °C in oil bath with continuous stirring (Scheme 1) [9]. The pH was adjusted to 7.0 using saturated $NaHCO_3$ solution after complete dissolution. The temperature was then raised to 90 °C after the addition of 0.09 mL ethanolamine. Equimolar quantity of the corresponding aldehyde solution in 1–2 mL EtOH was then added drop-wise with continuous stirring. The reaction was kept under reflux for approximately 5–8 h. The reaction was monitored by TLC every hour till a yellow or white precipitate was formed. After complete depletion of the starting aldehyde, the mixture was cooled and the precipitate was filtered and washed with EtOH–H_2O (1:5) before recrystallization from EtOH.

4.2.1. (Z)-5-(3-methoxy-4-(2-oxo-2-(pyrrolidin-1-yl)ethoxy) benzylidene)imidazolidine-2,4-dione (**5**)

Compound **5** was prepared according to the abovementioned procedure to afford 0.244 g, brown powder (70.7% yield). ^1H NMR (DMSO-d_6, 400 MHz) δ 1.76 (m, 2H), 1.88 (m, 2H), 3.31 (m, 2H), 3.46 (m, 2H), 3.85 (s, 3H), 4.75 (s, 3H), 6.39 (s, 1H), 6.85 (d, 1H, $J = 9.2$), 7.12 (d, 1H, $J = 9.2$), 7.14 (s, 1H), 10.81 (brs, 2H). ^{13}C NMR (DMSO-d_6, 100 MHz) δ 24.1 (CH_2), 26.7 (CH_2), 45.3 (CH_2), 46.2 (CH_2), 56.3 (CH_3), 67.1 (CH_2), 109.7 (CH), 113.3 (CH), 113.7 (CH), 123.3 (CH), 126.6 (qC), 126.8 (qC), 148,7 (qC), 149.4 (qC), 156.4 (qC), 166.0 (qC), 166.2 (qC); HREIMS *m/z* 344.1263 $[M-H]^+$ (calcd for $C_{17}H_{18}N_3O_5$, 344.1252).

4.2.2. (Z)-5-(2,4-dipropoxybenzylidene)imidazolidine-2,4-dione (**6**)

Nearly 0.273 g of **5** was prepared as a brown powder (89.8% yield). ^1H NMR (DMSO-d_6, 400 MHz) δ 0.98 (m, 6H), 2.51 (m, 4H), 3.97 (m, 4H), 6.53 (dd, 1H, $J = 2.2, 8.8$), 6.57 (d, 2H, $J = 2.2$), 6.66 (s, 1H), 7.54 (d, 1H, $J = 8.8$), 10.21 (brs, 1H), 11.11 (brs, 1H). ^{13}C NMR (DMSO-d_6, 100 MHz) δ 11.0 (CH_3), 11.1 (CH_3), 22.5 (CH_2), 22.6 (CH_2), 69.7 (CH_2), 70.1 (CH_2), 99.9 (CH), 103.7 (CH), 106.6 (CH), 114.8 (qC), 126.5 (qC), 130.7 (CH), 156.0 (qC), 158.6 (qC), 161.1 (qC), 166.2 (qC). HREIMS *m/z* 303.1355 $[M-H]^+$ (calcd for $C_{16}H_{19}N_2O_4$, 303.1345).

*4.2.3. (Z)-5-(3-methoxy-4-(2-oxo-2-phenylethoxy)benzylidene) imidazolidine-2,4-dione (**7**)*

Compound **7** was prepared to afford 0.202 g, yellow powder (57% yield). ^{1}H NMR (DMSO-d_6, 400 MHz) δ 3.87 (s, 3H), 5.60 (s, 2H), 6.37 (s, 1H), 6.86 (d, 1H, J = 8.8), 7.09 (dd, 1H, J = 1.8, 8.4), 7.13 (d, 1H, J = 2.2), 7.51 (m, 1H), 7.56 (dd, 1H, J = 7.7, 7.7), 7.67 (d, 1H, J = 7.3), 7.80 (m, 1H), 7.99 (d, 1H, J = 7.0),. ^{13}C NMR (DMSO-d_6, 100 MHz) δ 56.3 (CH_3), 70.9 (CH_2), 109.8 (CH), 112.8 (CH), 113.0 (CH), 123.2 (CH), 126.7 (qC), 126.9 (qC), 128.4 (CH), 129.5 (CH), 134.5 (qC), 134.7 (CH), 148.4 (qC), 149.4 (qC), 156.5 (qC), 166.4 (qC), 195.1 (qC). HREIMS m/z 351.1000 $[M-H]^+$ (calcd for $C_{19}H_{15}N_2O_5$, 351.0986).

*4.2.4. (Z)-5-(3-methoxy-4-(2-morpholino-2-oxoethoxy) benzylidene)imidazolidine-2,4-dione (**8**)*

Compound **8** was prepared to afford 0.243 g, white powder (66.7% yield). ^{1}H NMR (DMSO-d_6, 400 MHz) δ 3.45 (dd, 4H, J = 4.2, 11.9), 3.57 (dd, 4H, J = 4.2, 18.3), 3.85 (s, 3H), 4.87 (s, 2H), 6.38 (s, 1H), 6.88 (d, 1H, J = 8.8), 7.14 (m, 1H), 7.15 (m, 1H), 10.82 (brs, 1H) . ^{13}C NMR (DMSO-d_6, 100 MHz) δ 40.3 (CH_2), 56.2 (CH_3), 60.2 (CH_2), 68.2 (CH_2), 110.5 (CH), 113.5 (CH), 117.5 (CH), 126.2 (CH), 126.3 (qC), 133.4 (qC), 148.3 (qC), 148.7 (qC), 153.2 (qC), 166.4 (qC) 167.6 (qC). HREIMS m/z 360.1206 $[M-H]^+$ (calcd for $C_{17}H_{18}N_3O_6$, 360.1201).

*4.2.5. (Z)-5-(3-bromo-5-methoxy-4-propoxybenzylidene) imidazolidine-2,4-dione (**10**)*

PMH **10** was prepared to afford 0.164 g, yellow powder (46.3% yield). ^{1}H NMR (DMSO-d_6, 400 MHz) δ 0.99 (t, 3H, J = 7.3), 1.70 (m, 2H), 3.88 (s, 3H), 6.35 (s, 1H), 7.20 (s, 1H), 7.15 (s, 1H), 10.99 (brs, 1H) . ^{13}C NMR (DMSO-d_6, 100 MHz) δ 11.1 (CH_3), 23.6 (CH_2), 56.8 (CH_3), 74.9 (CH_2), 107.5 (CH), 114.0 (CH), 117.9 (qC), 125.5 (CH), 128.6 (qC), 130.7 (qC), 145.5 (qC), 153.9 (qC), 156.4 (qC), 166.0 (qC). HREIMS m/z 355.0252 $[M+H]^+$ (calcd for $C_{14}H_{16}BrN_2O_4$, 355.0293).

*4.2.6. (Z)-5-(4-(isopentyloxy)benzylidene)imidazolidine-2,4-dione (**11**)*

Compound **11** was prepared to afford 0.240 g, white powder (87.6% yield). ^{1}H NMR (DMSO-d_6, 400 MHz) δ 0.94 (d, 6H, J = 6.6), 1.61 (m, 2H), 1.78 (m, 1H), 4.03 (t, 2H, J = 6.6), 6.38 (s, 1H), 6.95 (d, 2H, J = 8.8), 7.57 (d, 2H, J = 8.8), 10.50 (brs, 1H), 11.18 (brs, 1H). ^{13}C NMR (DMSO-d_6, 100 MHz) δ 24.1 (CH_3), 24.9 (CH), 38.2 (CH_2), 65.0 (CH_2), 108.7 (CH), 126.1 (CH), 127.8 (qC), 129.9 (qC), 130.4 (CH), 155.3 (qC), 156.9 (qC), 166.0 (qC). HREIMS m/z 273.1244 $[M-H]^+$ (calcd for $C_{15}H_{17}N_2O_3$, 273.1239).

*4.2.7. (Z)-5-(2-methoxy-4-propoxybenzylidene)imidazolidine-2,4-dione (**14**)*

Compound **14** was prepared to afford 0.211 g, yellow powder (76.5% yield). ^{1}H NMR (DMSO-d_6, 400 MHz) δ 0.99 (t, 3H, J = 7.0), 1.73 (m, 2H), 3.87 (s, 3H), 4.04 (t, 2H, J = 6.4), 6.29 (s, 1H), 6.55 (m, 1H), 6.56 (m, 1H), 8.02 (d, 1H, J = 8.8), 10.76 (brs, 1H), 11.17 (brs, 1H). ^{13}C NMR (DMSO-d_6, 100 MHz) δ 10.2 (CH_3), 22.9 (CH_2), 56.8 (CH_3), 70.3 (CH_2), 103.2 (CH), 106.3 (CH), 107.7 (qC), 123.2 (CH), 124.7 (qC), 131.7 (CH), 144.2 (qC), 153.8 (qC), 156.2 (qC), 166.1 (qC); HREIMS m/z 277.1109 $[M+H]^+$ (calcd for $C_{14}H_{17}N_2O_4$, 277.1188).

*4.2.8. (Z)-5-(4-tert-butoxy-3-chloro-2-methoxybenzylidene) imidazolidine-2,4-dione (**15**)*

Compound **15** was prepared to afford 0.131 g, white powder (40.4% yield). ^{1}H NMR (DMSO-d_6, 400 MHz) δ 1.41 (s, 9H), 3.83 (s, 3H), 6.72 (s, 1H), 6.84 (d, 1H, J = 8.8), 7.89 (d, 1H, J = 8.8), 10.55 (brs, 1H), 11.06 (brs, 1H). ^{13}C NMR (DMSO-d_6, 100 MHz) δ 27.7 (CH_3), 59.8 (CH_3), 77.8 (qC), 104.4 (CH), 108.0 (qC), 108.2 (qC), 122.5 (CH), 124.1 (qC), 128.7 (CH), 150.2 (qC), 154.8 (qC), 156.2 (qC), 166.0 (qC); HREIMS m/z 325.0889 $[M+H]^+$ (calcd for $C_{15}H_{18}ClN_2O_4$, 325.0955).

*4.2.9. (Z)-5-(3-chloro-2,6-dimethoxy-4-propoxybenzylidene) imidazolidine-2,4-dione (**16**)*

Compound **16** was prepared to afford 0.172 g, orange powder (50.6% yield). ^{1}H NMR (DMSO-d_6, 400 MHz) δ 0.97 (t, 3H, J = 7.2), 1.73 (m, 2H), 3.88 (s, 3H), 4.01 (t, 2H, J = 6.6), 6.16 (s, 1H), 6.82 (s, 1H), 10.65 (brs, 1H), 11.23 (brs, 1H). ^{13}C NMR (DMSO-d_6, 100 MHz) δ 10.5 (CH_3), 22.8 (CH_2), 55.9 (CH_3), 60.1 (CH_3), 74.3 (CH_2), 96.3 (CH), 100.0 (qC), 102.2 (qC), 122.1 (CH), 124.8 (qC), 152.9 (qC), 154.4 (qC), 155.1 (qC), 157.2 (qC) 166.3 (qC); HREIMS m/z 341.1008 $[M+H]^+$ (calcd for $C_{15}H_{18}ClN_2O_5$, 341.0904).

*4.2.10. (Z)-5-(4-tert-butoxybenzylidene)imidazolidine-2,4-dione (**17**)*

Compound **17** was prepared to afford 0.227 g, white powder (83.4% yield). ^{1}H NMR (DMSO-d_6, 400 MHz) δ 1.37 (s, 9H), 6.53 (s, 1H), 7.05 (d, 2H, J = 8.4), 7.46 (d, 2H, J = 8.4), 10.53 (brs, 1H), 11.03 (brs, 1H). ^{13}C NMR (DMSO-d_6, 100 MHz) δ 27.9 (CH_3), 78.9 (qC), 110.1 (CH), 123.7 (CH), 127.7 (qC), 128.2 (qC), 129.9 (CH), 156.2 (qC), 166.1 (qC); HREIMS m/z 259.1084 $[M-H]^+$ (calcd for $C_{14}H_{15}N_2O_3$, 259.1088).

*4.2.11. (Z)-5-((4-methyl-1H-imidazol-5-yl)methylene) imidazolidine-2,4-dione (**19**)*

Compound **19** was prepared to afford 0.118 g, yellow powder (61.5% yield). ^{1}H NMR (DMSO-d_6, 400 MHz) δ 2.29 (s, 3H), 6.39 (s, 1H), 7.76 (s, 1H), 9.59 (brs, 1H), 11.03 (brs, 1H). ^{13}C NMR (DMSO-d_6, 100 MHz) δ 9.6 (CH_3), 101.0 (CH), 126.0 (qC), 129.6 (qC), 132.7 (qC), 134.6 (CH), 154.2 (qC), 165.4 (qC); HREIMS m/z 193.0729 $[M+H]^+$ (calcd for $C_8H_9N_4O_2$, 193.0720).

*4.2.12. (Z)-5-((3H-pyrrolo[2,3-b]pyridin-3-yl)methylene) imidazolidine-2,4-dione (**20**)*

Compound **20** was prepared to afford 0.135 g, yellow powder (59.2% yield). ^{1}H NMR (DMSO-d_6, 400 MHz) δ 6.73 (s, 1H), 7.16 (dd, 1H, J = 4.8, 8.1), 8.24 (s, 1H), 8.25 (m, 1H), 8.28 (d, 1H, J = 4.8), 8.31 (s, 1H), 10.24 (brs, 1H), 11.07 (brs, 1H). ^{13}C NMR (DMSO-d_6, 100 MHz) δ 79.7 (qC), 101.5 (CH), 107.8 (qC), 117.0 (CH), 119.7 (qC), 125.0 (qC), 127.5 (CH), 144.3 (CH), 148.9 (qC), 155.9 (qC), 165.9 (qC); HREIMS m/z 252.0750 $[M]^+$ (calcd for $C_{12}H_{11}N_3O_2Na$, 252.0743).

*4.2.13. (Z)-5-((6-(thiophen-2-yl)pyridin-2-yl)methylene) imidazolidine-2,4-dione (**21**)*

Compound **21** was prepared to afford 0.164 g, brown powder (53.9% yield). ^{1}H NMR (DMSO-d_6, 400 MHz) δ 6.50 (s, 1H), 7.21 (d, 1H, J = 3.6), 7.49 (dd, 1H, J = 3.6, 4.8), 7.72 (d, 1H, J = 5.2), 7.84 (s, 3H), 8.31 (s, 1H), 9.99 (brs, 1H), 11.02 (brs, 1H). ^{13}C NMR (DMSO-d_6, 100 MHz) δ 104.8 (CH), 118.1 (CH), 124.9 (CH), 126.7 (CH), 129.0 (CH), 129.5 (CH), 132.6 (qC), 138.9 (CH), 144.3 (qC), 151.8 (qC), 153.9 (qC), 154.9 (qC), 165.6 (qC); HREIMS m/z 270.0336 $[M-H]^+$ (calcd for $C_{13}H_8N_3O_2S$, 270.0343).

*4.2.14. (Z)-5-(benzo[d][1,3]dioxol-4-ylmethylene)imidazolidine-2,4-dione (**22**)*

Compound **22** was prepared to afford 1.67 g, white powder (72% yield). ^{1}H NMR (DMSO-d_6, 400 MHz) δ 6.12 (s, 2H), 6.31 (s, 1H), 6.87 (dd, 1H, J = 1.5, 7.7), 6.90 (dd, 1H, J = 8.0, 7.7), 8.12 (dd, 1H, J = 8.0, 1.5) 10.22 (s, 1H), 11.30 (s, 1H). ^{13}C NMR (DMSO-d_6, 100 MHz) δ 99.8 (CH_2), 114.7 (CH), 116.2 (qC), 120.8 (CH), 121.9 (CH), 122.4 (CH), 124.7 (qC), 147.2 (qC), 147.1 (qC), 158.7 (qC), 162.5 (qC); HREIMS m/z 255.0380 $[M+Na]^+$ (calcd for $C_{11}H_8N_2O_4Na$, 255.0376).

*4.2.15. (Z)-5-(indolin-7-ylmethylene)imidazolidine-2,4-dione (**23**)*

Compound **23** was prepared to afford 0.102 g, white powder (44.5% yield). ^{1}H NMR (DMSO-d_6, 400 MHz) δ 2.50 (m, 2H), 4.39 (t, 2H, J = 8.8), 6.59 (s, 1H), 7.13 (dd, 1H, J = 7.7, 7.3), 7.25 (d, 1H, J = 7.3), 8.43 (s, 1H), 8.52 (s, 1H), 10.72 (brs, 1H), 11.02 (brs, 1H). ^{13}C NMR

(DMSO-d_6, 100 MHz) δ 27.4 (CH_2), 47.9 (CH_2), 114.0 (CH), 117.4 (qC), 122.3 (CH), 122.9 (CH), 124.1(CH), 130.8 (qC), 132.3 (qC), 135.2 (qC), 156.5 (qC), 156.9 (qC); HREIMS m/z 252.0750 $[M+Na]^+$ (calcd for $C_{12}H_{11}N_3O_2Na$, 252.0743).

4.2.16. (Z)-5-((6-methoxypyridin-2-yl)methylene)imidazolidine-2,4-dione (**24**)

Compound **24** was prepared to afford 0.161 g, yellow powder (73.5% yield). ^{1}H NMR (DMSO-d_6, 400 MHz) δ 3.99 (s, 3H), 6.44 (s, 1H), 6.75 (d, 1H, $J = 8.0$), 7.22 (d, 1H, $J = 7.3$), 7.73 (dd, 1H, $J = 7.3$, 8.0), 9.62 (brs, 1H), 11.47 (brs, 1H). ^{13}C NMR (DMSO-d_6, 100 MHz) δ 53.8 (CH_3), 106.1 (CH), 110.7 (CH), 119.8 (CH), 131.5 (qC), 140.5 (CH), 151.7(qC), 154.9 (qC), 163.7 (qC), 165.6 (qC); HREIMS m/z 218.0563 $[M-H]^+$ (calcd for $C_{10}H_8N_3O_3$, 218.0566).

4.2.17. (Z)-5-((1H-imidazol-5-yl)methylene)imidazolidine-2,4-dione (**25**)

Compound **25** was prepared to afford 0.091 g, yellow powder (51.1% yield). ^{1}H NMR (DMSO-d_6, 400 MHz) δ 6.41 (s, 1H), 7.59 (s, 1H), 7.86 (s, 1H), 9.68 (brs, 1H), 11.17 (brs, 1H). ^{13}C NMR (DMSO-d_6, 100 MHz) δ 102.2 (CH), 123.1 (qC), 131.1 (qC), 135.5 (CH), 136.7 (qC), 154.2 (qC), 165.7 (qC), 165.6 (qC); HREIMS m/z 179.0551 $[M+H]^+$ (calcd for $C_7H_6N_4O_2$, 179.0579).

4.2.18. (Z)-5-((4-iodo-1H-pyrrol-2-yl)methylene)imidazolidine-2,4-dione (**27**)

Compound **27** was prepared to afford 0.253 g, white powder (83.8% yield). ^{1}H NMR (DMSO-d_6, 400 MHz) δ 6.46 (s, 1H), 6.69 (s, 1H), 748 (s, 1H), 10.45 (bs, 1H), 10.92 (bs, 1H). ^{13}C NMR (DMSO-d_6, 100 MHz) δ 108.8 (CH), 109.2(CH), 111.2 (qC), 119.0 (CH), 129.2.5 (qC), 131.7(qC), 154.7 (qC), 165.2 (qC); HREIMS m/Hz 303.95710 $[M+H]^+$ (calcd for $C_8H_6IN_3O_2$, 303.9583).

4.3. Cell culture

Prostate cancer cell line PC-3 was purchased from ATCC (Manassas, VA). The cell line was grown in 10% fetal bovine serum (FBS) and RPMI 1640 (GIBCO-Invitrogen, NY) supplemented with 2 mmol/L glutamine, 100 μg/mL penicillin G, and 100 μg/mL streptomycin, at 37 °C under 5% CO_2.

4.4. MTT proliferation assay

The growth of PC-3 cancer cell lines was measured using MTT kit (TACS™, TREVIGEN®, Inc.) [32,33]. Exponentially growing cells were plated in a 96 well plate at a density of 8×10^3 cells per well, and allowed to attach for 24 h. Complete growth medium was then replaced with 100 μL of RPMI of serum free medium (GIBCO-Invitrogen, NY) containing 200 μM of the specific tested PMH and culture continued at 37 °C under 5% CO_2. After 72 h of culture, the cells were treated with MTT solution (10 μL/well) at 37 °C for 4 h. The color reaction was stopped by the addition of solubilization/stop solution (100 μL/well), and the incubation at 37 °C continued to completely dissolve the formazan product. Absorbance of the samples was determined at 570 nm with an ELISA plate reader (BioTek, VT). The number of cells per well was calculated against a standard curve prepared by plating various concentration of cells, as determined by hemocytometer, at the start of each experiment.

4.5. Cultrex® cell invasion assay

Anti-invasive activities were measured using Trevigen's Cultrex® Cell Invasion Assay as previously described [28,29]. About 50 μL of basement membrane extract (BME) coat was added per well. After incubation for 4 h at 37 °C in a 5% CO_2, 50,000 cells/50 μL of PC-3 cells in serum free RPMI medium were added per well to the top chamber containing the tested PMH (50 μM). About 150 μL of RPMI medium was then added to the lower chamber containing 10% FBS and penicillin/streptomycin and using fibronectin (1 μL/mL) and *N*-formyl-met-leu-phe (10 nM) as chemoattractants. Cells were allowed to migrate to lower chamber at 37 °C in CO_2 incubator. After 24 h, top and bottom chambers were aspirated and washed with washing buffer supplemented with the kit. About 100 μL of Cell Dissociation Solution/Calcein-AM solution was added to the bottom chamber and incubated at 37 °C in CO_2 incubator for 1 h. The cells internalize calcein-AM, and the intracellular esterases cleaved the AM moiety to generate free calcein. Fluorescence of the samples was determined at 485 nm excitation, 520 nm emission, using ELISA plate reader (BioTek, VT). The number of cells that have invaded through the BME coat was calculated using a standard curve.

4.6. Wound-healing assay

Cells were plated onto sterile 24-well plates and allowed to recover for a confluent cell monolayer formed in each well (>90% confluence). Wounds were then inflicted to each cell monolayer using a sterile 200 μL pipette tip. Media were removed, cell monolayers were washed once with PBS, and then fresh media containing test compounds were added to each well. Test compounds were prepared in DMSO at different concentrations and added to the plates, each in triplicate using DMSO as a vehicle control. The incubation was carried out for 24 h under serum-starved conditions, after which media was removed and cells were fixed and stained using Diff-Quick staining (Dade Behring Diagnostics). The number of cells migrated on the scratched wound were counted under the microscope in three or more randomly selected fields (magnification: 400×). Final results are expressed as mean ± SEM per 400× field. All treatments, including the controls, were documented photographically. IC_{50} for each compound was calculated using nonlinear regression (curve fit) of log concentration versus the number of cells/well implemented using GraphPad Prism 5.0 (GraphPad Software, La Jolla, CA).

4.7. Determination of the ^{13}C NMR chemical Shift at the β-carbon (C5)

The ^{13}C NMR chemical shift of the β-carbon was used to identify the electronic influence of the substituents at the phenyl ring. The difference in the chemical shift $\Delta\delta$ was given by ($\delta_H - \delta_R$), where δ_R is the carbon chemical shift of the substituted phenylmethylene hydantoin and δ_H is that of the unsubstituted compound. The $\Delta\delta$ value is known to be sensitive to the electronic influence of the substituents on the aryl moieties [34,35].

4.8. Molecular modeling

Three-dimensional structure building and all modeling were performed using the SYBYL program package [30], version 8.0, installed on DELL desktop workstations equipped with a dual 2.0 GHz Intel® Xeon® processor running the Red Hat Enterprise Linux (version 5) operating system. Energy minimizations were performed using the Tripos force field with a distance-dependent dielectric and the Powell conjugate gradient algorithm with a convergence criterion of 0.01 kcal/(mol A) [36]. Partial atomic charges were calculated using the semiempirical program MOPAC 6.0 and applying the AM1 [37] before calculating their physicochemical properties. Size, electronic, and lipophilic properties were theoretically calculated using the SYBYL 8.0 spreadsheet autofill module. The multivariate analyses were performed with JMP 8.0 (SAS Institute Inc.) using the default settings.

Appendix. Supplementary material

Supplementary data associated with this article can be found in the online version, at doi:10.1016/j.ejmech.2010.08.066.

References

[1] A. Jemal, R. Rebecca Siegel, E. Ward, Y. Hao, J. Xu, M. Thun, Cancer J. Clin. 59 (2009) 225–249.
[2] I.M. Thompson, P.J. Goodman, C.M. Tangen, M.S. Lucia, G.J. Miller, L.G. Ford, M.M. Lieber, R.D. Cespedes, J.N. Atkins, S.M. Lippman, S.M. Carlin, A. Ryan, C.M. Szczepanek, J.J. Crowley, C.A. Coltman Jr., New Engl. J. Med. 349 (2003) 215–224.
[3] T. Makinen, T.L. Tammela, M. Hakama, U.H. Stenman, S. Rannikko, J. Aro, H. Juusela, L. Maattanen, A. Auvinen, Clin. Cancer Res. 9 (2003) 2435–2439.
[4] L. Bubendorf, A. Schopfer, U. Wagner, G. Sauter, H. Moch, N. Willi, T.C. Gasser, M.J. Mihatsch, Hum. Pathol. 31 (2000) 578–583.
[5] M. Bolla, L. Collette, L. Blank, P. Warde, J.B. Dubois, R.O. Mirimanoff, G. Storme, J. Bernier, A. Kuten, C. Sternberg, J. Mattelaer, J. Lopez Torecilla, J.R. Pfeffer, C. Lino Cutajar, A. Zurlo, M. Pierart, Lancet 360 (2002) 103–106.
[6] A.V. D'Amico, J. Manola, M. Loffredo, A.A. Renshaw, A. DellaCroce, P.W. Kantoff, J. Am. Med. Assoc. 292 (2004) 821–827.
[7] D.R. Shepard, D. Raghavan, Nat. Rev. Clin. Oncol. 7 (2010) 13–21.
[8] J.C. Cheville, D. Tindall, C. Boelter, R. Jenkins, C.M. Lohse, V.S. Pankratz, T.J. Sebo, B. Davis, M.L. Blute, Cancer 95 (2002) 1028–1036.
[9] J.C. Thenmozhiyal, P.T. Wong, W.K. Chui, J. Med. Chem. 47 (2004) 1527–1535.
[10] M. Meuesel, M. Gutschow, Org. Prep. & Procedures Int. 36 (2004) 391–443.
[11] B. Gabos, M. Munck Af Rosenschoeld, L. Ripa, WO 2009007747 A2 20090115, PCT Int. Appl. (2009).
[12] L. Naohiro, S. Tadayoshi, K. Ikuo, Y. Katsuji, A. Yutaka, Y. Toshiaki, Jpn. Kokai Tokkyo Koho (1987) JP 62029570 A 19870207.
[13] P. Shapiro, A.D. Mackerell, WO 2006105237 A2 20061005, PCT Int. Appl. (2006).
[14] W. Koenig, G. Zoller M. Just, B. Jablonka, DE 4126277 A1 19930211, Ger. Offen. (1993).
[15] A.H. Abadi, B.D. Gary, H.N. Tinsley, G.A. Piazza, M. Abdel-Halim, Eur. J. Med. Chem. 45 (2010) 1278–1286.
[16] V. Zuliani, C. Carmi, M. Rivara, M. Fantini, A. Lodola, F. Vacondio, F. Bordi, P.V. Plazzi, A. Cavazzoni, M. Galetti, R.R. Alfieri, P.G. Petronini, M. Mor, Eur. J. Med. Chem. 44 (2009) 3471–3479.
[17] C.S. Basappa, Ananda Kumar, S.N. Swamy, K. Sugahara, K.S. Rangappa, Bioorg. Med. Chem. 17 (2009) 4928–4934.
[18] S. Chen, N.J.S. Huby, N. Kong, J.A. Moliterni, O.J. Morales, WO 2009021887 A1 20090219, PCT Int. Appl. (2009).
[19] C.V. Kavitha, M. Nambiar, C.S. Ananda Kumar, B. Choudhary, K. Muniyappa, K.S. Rangappa, S.C. Raghavan, Biochem. Pharm. 77 (2009) 348–363.
[20] M.E. Jung, C.L. Sawyers, S. Ouk, C. Tran, J. Wongvipat, WO 2007126765 A2 20071108, PCT Int. Appl. (2007).
[21] (a) M.A. Khanfar, B. AbuAsal, M. Mudit, A. Kaddoumi, K.A. El Sayed, Bioorg. Med. Chem. 17 (2009) 6032–6039;
(b) K. Yang, Y. Tang, K.A. Iczkowski, Am. J. Transl. Res. 2(2010) 88–94.
[22] K.V. Sashidhara, K.N. White, P. Crews, J. Nat. Prod. 72 (2009) 588–603.
[23] K.H. Lee, J. Nat. Prod. 73 (2010) 500–516.
[24] D.J. Newman, G.M. Cragg, J. Nat. Prod. 70 (2007) 461–477.
[25] N. Fleshner, A.R. Zlotta, Cancer 110 (2007) 1889–1899.
[26] G.V. Shah, A. Muralidharan, S. Thomas, M. Gokulgandhi, M. Mudit, M. Khanfar, K.A. El Sayed, Mol. Cancer Ther. 8 (2009) 509–520.
[27] M. Mudit, M. Khanfar, A. Muralidharan, S. Thomas, G.V. Shah, R.W.M. van Soest, K.A. El Sayed, Bioorg. Med. Chem. 17 (2008) 1731–1738.
[28] K.P. Tamilarasan, G.K. Kolluru, M. Rajaram, M. Indhumathy, R. Saranya, S. Chatterjee, BMC Cell Biol. 7 (2006) 17–30.
[29] P.R. Borghesani, J.M. Peyrin, R. Klein, J. Rubin, A.R. Carter, P.M. Schwartz, A. Luster, G. Corfas, R.A. Segal, Development 6 (2002) 1435–1442.
[30] Tripos Associates, SYBYL Molecular Modeling Software, Version 8.0. Tripos Associates, St. Louis, MO, 2007. http://www.tripos.com.
[31] S. Wold, C. Albano, W.J. Dunn III, U. Edlund, K. Esbensen, P. Geladi, S. Hellberg, E. Johanson, W. Lindberg, M. Sjostrom, NATO Sci. Ser. C 138 (1984) 17–95.
[32] T. Mosmann, J. Immunol. Methods 65 (1983) 55–63.
[33] M.C. Alley, D.A. Scudiero, A. Monks, M.L. Hursey, M.J. Czerwinski, D.L. Fine, B.J. Abbott, J.G. Mayo, R.H. Shoemaker, M.R. Boyd, Cancer Res. 48 (1988) 589–601.
[34] G.N. Wernly Chung, J.M. Mayer, A. Tsantili-Kakoulidou, B. Testa, Int. J. Pharm. 63 (1990) 129–134.
[35] X. Rong, M.L. Go, Chem. Pharm. Bull. 45 (1997) 476–481.
[36] M. Clark, R.D. Cramer III, N. van Opdenbosch, Comput. Chem. 10 (1989) 982–1012.
[37] J.J. Stewart, J. Comput. Aided Mol. Des. 4 (1990) 1–105.